





Behavior of Reinforced HPFRCC Columns Subjected to Axial and Lateral Loads

Joseph A. Almeida¹, Matthew J. Bandelt Ph.D., P.E.¹

¹: New Jersey Institute of Technology, Newark, United States.

Abstract

While widely adopted prescriptive-based design practices work to limit the probability of complete collapse, relatively little attention and emphasis is placed on the damage levels and functionality of structures after seismic events. High-performance fiber reinforced cementitious composites reinforced with steel (R/HPFRCCs) have been of growing interest for such seismic applications to improve structural level damage and performance. In order to progress the implementation of these materials at the structural level, a systematic approach toward understanding the mechanics of R/HPFRCC columns is warranted. Therefore, in this study, an existing numerical framework for R/HPFRCC beams was extended to the analysis of columns across a range of materials, reinforcement ratios, and axial load levels to evaluate the change in component level response. It was observed that axial load can considerably increase the nominal bending moment capacity of R/HPFRCC columns as well as affect the drift capacity. A shift from failure on the tension side of the element (e.g., reinforcement fracture) to the compression side (e.g., crushing of the HPFRCC) of the numerically tested column occurred between an axial load ratio of 10 and 20%. Lastly, changes in bond stress due to the material level tensile strength were shown to considerably impact the ultimate component drift capacity.

Keywords

High-Performance Fiber Reinforced Cementitious Composite, UHPC, ECC, column, axial load, failure mechanisms, finite element, simulation







1 Introduction

The design of seismic structural components following displacement-based methods often entails reinforcement detailing such that sufficient inelastic deformation and strength capacities are provided (Paulay & Priestley, 1992). While widely adopted prescriptive-based design practices work to limit the probability of complete collapse, relatively little attention and emphasis is placed on the damage levels and functionality of structures after seismic events. The concurrent development and research into high-performance fiber-reinforced cementitious composites reinforced with steel (R/HPFRCCs) have been of growing interest for such seismic applications (Shao et al., 2022) to enhance the mechanical and damage performance of structures (Tariq et al., 2021). HPFRCCs derive their enhanced performance through the addition of small discontinuous fibers that result in pseudo-strain hardening and multiple microcracking behaviors under tension (Naaman & Reinhardt, 2006). To date, considerable design guidance for HPFRCC and FRC flexural components have been developed in contrast to axially loaded components (ACI Committee 544, n.d.; Russell & Graybeal, 2013). As a result, the lack of understanding of the mechanics of R/HPFRCC columns warrants further investigation in order to progress the implementation of HPFRCC materials and understand its' structural level behavior (Tariq et al., 2021).

Experimental testing of R/HPFRCC columns has been reported across a range of HPFRCC materials, section geometries, and reinforcement configurations (Aboukifa & Moustafa, 2021; Chao et al., 2021; Marchand et al., 2019; Wu et al., 2017; Xu et al., 2017). These studies have highlighted the higher strength and deformation capacity, damage tolerance, and energy dissipation potential of R/HPFRCC columns. For example, in a study by (Chao et al., 2021), a reinforced concrete column with Ultra High-Performance Concrete (UHPC) cast in the plastic hinge region was tested and compared to a fully reinforced concrete column. The peak base shear and drift capacity before considerable strength degradation were observed to be 15% and 1.55 times greater in the UHPC column compared to the full concrete column respectively. Further, significantly lower damage levels were observed in the UHPC column in comparison to the full reinforced concrete column. In a series of column tests conducted by Hung et al., (2018), the effects of fiber reinforcement percentages and transverse reinforcement ratio were investigated. Hung et al., (2018) found that the addition of as little as 0.75% fiber reinforcement by volume can limit spalling damage in addition to preventing the buckling of longitudinal reinforcement.

The use of HPFRCC materials in columns appears promising but a systematic approach to understand the effects of various design parameters on column response must be made. Therefore, in this study, an existing numerical framework for R/HPFRCC beams is extended to the analysis of columns across a range of materials, reinforcement ratios, and axial load levels and is described in the following sections.

2 Numerical Modeling Setup

Recent developments in HPFRCC material models have resulted in numerical simulations capable of capturing experimentally observed component responses and failure mechanisms (Bandelt & Billington, 2018; Shao et al., 2021). This numerical framework has enabled researchers to extend their investigations beyond experimental studies to specifically target system variables







and investigate their significance (Pokhrel & Bandelt, 2019; Shao & Billington, 2022). Building off these works, a series of twelve two-dimensional numerical simulations were carried out in a commercially available finite element software, DIANA FEA 10.5. An orthogonal test matrix of three factors (i.e., variables) with two to three levels was used to investigate the impact of different HPFRCC material properties, reinforcement ratios, and axial load levels.

2.1 Model geometry

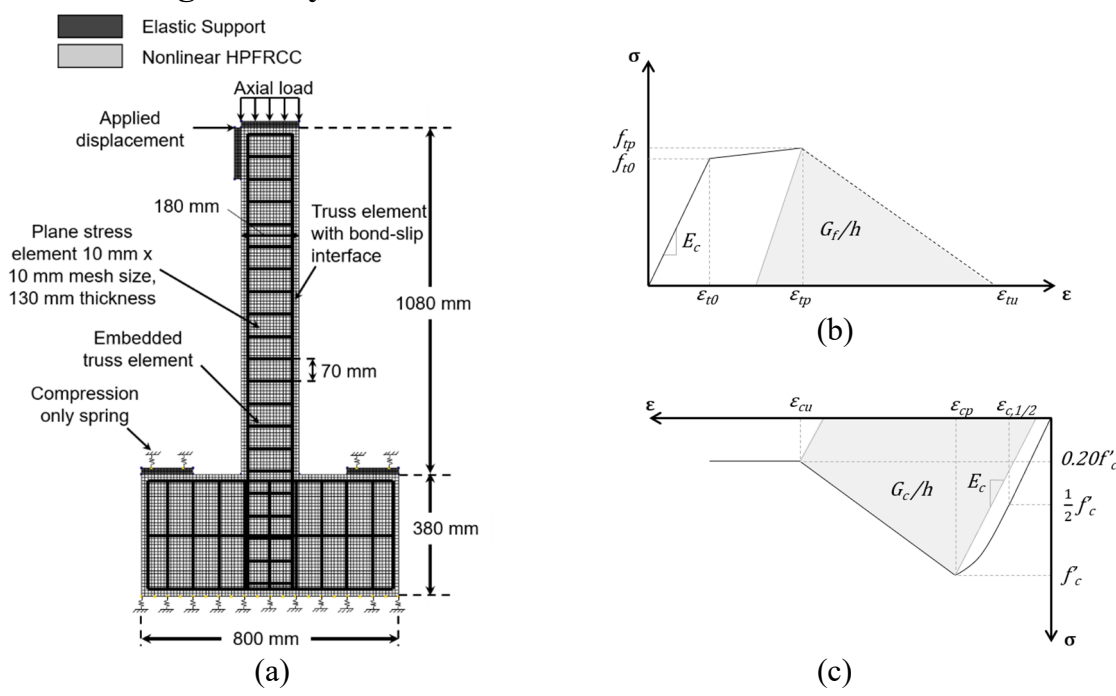


Figure 1: (a) Column finite element model, (b) uniaxial tension model adapted from (Shao et al., 2021), and (c) uniaxial compression model adapted from (Shao et al., 2021).

In Figure 1a., the column geometries, boundary conditions, and loading scenario of the numerical models are illustrated. The column geometries were selected to represent the scale range of future experimental column tests and were thus limited by the loading capacity of the laboratory equipment. Therefore, the section dimensions of 180 mm \times 130 mm $(h \times b)$ were selected. A shear span length (L_s) , defined herein as the length of the column from the column-base interface to the lateral load application point, of 1080 mm was selected and corresponds to an aspect ratio (L_s/h) of 6. A foundation beam with dimensions of 800 mm \times 130 mm \times 380 mm $(h \times b \times l)$ was provided. In order to avoid concentrated damage, elastic steel plates were modeled at the loading and column anchorage locations. Subsequently, the column, foundation beam, and steel plates were discretized into 10 mm \times 10 mm \times 130 mm plane-stress quadrilateral elements with a 3 \times 3 Gaussian integration scheme.

The R/HPFRCC columns were symmetrically reinforced on both sides either with two 10mm or two 13mm mild longitudinal steel bars representing a reinforcement ratio ($\rho = A_{s,tension}/b \cdot d$) of 0.70% and 1.25% respectively. Since the effects of varying transverse reinforcement were not within the scope of this study, a minimum transverse reinforcement ratio ($A_{sh}/s \cdot b$) per ACI 318-19 of 0.18% was fixed across all simulations. Steel reinforcements were also discretized into 10 mm long embedded truss elements.







2.2 Constitutive material models

As previously mentioned, recent advancements have been made regarding HPFRCC material constitutive models allowing for tension, compression, and bond-slip responses to be largely derived from basic engineering parameters (Bandelt & Billington, 2016a; Shao et al., 2021; Shao & Ostertag, 2022; Wille et al., 2014). In this study, the basic and a few advanced engineering properties reported in the literature for ECC and UHPC were used to derive the full material responses and are summarized in Table 1.

Table 1: Assumed HPFRCC material properties

	Notation	Unit	ECC	UHPC
Modulus of Elasticity	E	[MPa]	18500	40310
Tensile strength	f_t	[MPa]	2.9	8
Strain at the onset of tensile softening	$arepsilon_{tp}$	[mm/mm]	0.0075	0.002
Tensile fracture energy	G_f	[N/mm]	6.1	19
Compressive strength	f'_c	[MPa]	55	120
Strain at peak compressive stress	$arepsilon_{cp}$	[mm/mm]	0.00489	0.0038
Compressive fracture energy	G_c	[N/mm]	138	180
Max bond stress	$ au_{max}$	[MPa]	8.9	18.79

Table 2: Assumed steel reinforcement properties

	Notation	Unit	No. 3	No. 10 & No.13
Modulus of Elasticity	$E_{\scriptscriptstyle S}$	[MPa]	205000	200000
Yield stress	$f_{\mathcal{Y}}$	[MPa]	445	455
Ultimate stress	f_u	[MPa]	690	675
Ultimate strain	$arepsilon_u$	[mm/mm]	0.18	0.18

Using reported HPFRCC properties from Moreno et al. (2014), Graybeal (2006), and Willie & Naaman (2010), the tensile response was calculated using an idealized trilinear stress-strain envelope whose softening state was normalized by the tensile fracture energy and element height as shown in Figure 1b. In addition, to capture the effects of HPFRCC tension cracking, a total strain-based smeared crack model was employed with a fixed crack orientation (Rots, 1988).

To model the HPFRCC compressive response, reported compressive strengths were used in combination with the multi-linear stress-strain rules developed by Shao et al., (2021). The compressive softening state was normalized by the compressive fracture energy and element height and an overview of the adopted model is illustrated in Figure 2c. In the context of this paper, the term "unconfined" represents the compression stress-stress behavior – including the inherent confinement due to fibers – of the HPFRCC materials with no transverse reinforcement.

Previous studies investigating the tension stiffening and bond behavior of R/HPFRCCs have highlighted its impact on plastic strain distribution in reinforcement as well as the maximum displacement capacity of components (Bandelt & Billington, 2018; Moreno et al., 2014).







Therefore, a Von Mises plasticity model using the material properties in Table 2 with bond-slip laws for ECC and UHPC was implemented (Bandelt & Billington, 2016a; Shao & Ostertag, 2022).

2.3 Boundary and loading conditions

To account for typical experimental boundary conditions, compression-only springs were modeled at the steel anchorage plates and foundation beam. Loading of the column was accomplished in two stages. Stage one entailed the application of a distributed line load at an axial load level $(P/f'_c \cdot A_g)$ corresponding to 0%, 10%, or 20%. Subsequently, a lateral displacement of 0.25 mm was applied in a monotonic stepwise manner.

2.4 Numerical analysis methods

A Newton-Raphson iterative method with a line-search algorithm was employed to solve for equilibrium. Each iterative step was considered converged when a displacement norm of 1%, force norm of 1%, and energy norm of 0.1% were met.

3 Numerical results and discussion

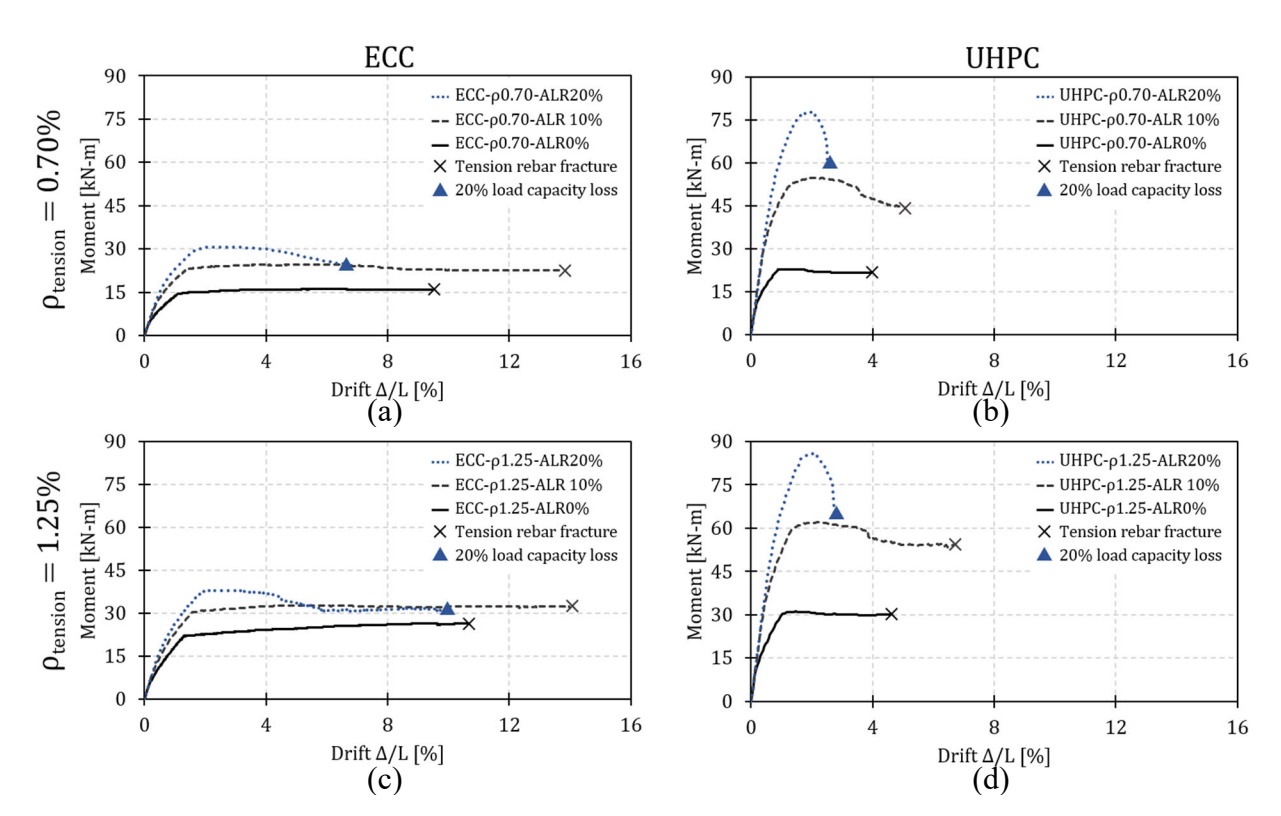


Figure 2: Bending moment versus drift responses at various axial load ratios (ALR) and tension reinforcement ratios. (a) ECC at $\rho = 0.70\%$, (b) UHPC at $\rho = 0.70\%$, (c) ECC at $\rho = 1.25\%$, and (d) UHPC at $\rho = 1.25\%$.

Note in the subsequent paragraphs each individual simulation is identified using the following notation, HPFRCC material-reinforcement ratio-axial load ratio (e.g., ECC-p1.25-ALR0%).







A comparison between ECC's and UHPC's bending moment ($M_{bending} = P \cdot L_s$) versus drift capacities ($\frac{\Delta_{load\ point}}{L_s}$), as shown in Figure 2a-d., reveals the effects of material-level behavior and axial load levels on component responses. For example, in Figures 2a and 2b., the nominal bending moment capacity of UHPC- ρ 0.70-ALR-0% is 1.4 times higher than ECC- ρ 0.70-ALR-0%. As the axial load ratio increased to 10%, UHPC- ρ 0.70-ALR-10%'s nominal moment capacity increased to 2.2 times that of ECC. The observed increase in the bending moment capacity of UHPC over ECC with increasing axial load can largely be attributed to the increasing utilization of UHPC's high compression strength. This is due to the fact that as the axial load increases, the depth to the neutral axis increases and thus results in a greater compression area.

When comparing the relative increase in moment capacity at different axial load levels in Figure 2b., the rate at which the moment capacity increased was found to decrease with the axial load. This is due to the column becoming more compression-dominate and gradually approaching its' pure axial load capacity.

A shift from tension fracture (i.e., tension reinforcement reached a strain of 0.18 mm/mm) to a compression failure (i.e., 20% load capacity loss due to crushing of the cementitious material) was also found to coincide with increasing axial load. Both ECC and UHPC columns failed in tension at an axial load ratio of 0%. Similar, tension failure mechanisms in cantilever and simply supported ECC and UHPC beams have also been observed and aligned with the simulated column failure mechanism (Bandelt & Billington, 2016b; Frank et al., 2017; Shao & Billington, 2022; Yoo & Yoon, 2015). Increases in axial load levels to 10% were found to increase the column drift capacity while maintaining a tension failure mechanism. Failure mechanisms of axially loaded columns reported in the literature show the predominately observed failure mechanism is compression failure (Hung et al., 2018; Li et al., 2019; Wu et al., 2017; Xu et al., 2017). While full utilization of tension reinforcement prior to compression failure is often difficult to achieve, several UHPC column tests have reported progressive rebar fracture (Aboukifa & Moustafa, 2021; Chao et al., 2021; Marchand et al., 2019). Therefore, the potential to obtain favorable tension failure in axially loaded R/HPFRCC columns may be possible at low axial loads. Future investigation should attempt to identify the structural design limits to achieve the tension failure mechanism of low axially loaded columns. Lastly, further increases in the axial load level to 20% were found to decrease the column drift capacity as the column failure mechanism shifted to a compression failure.

In Figures 2c. and 2d., the effects of increasing the reinforcement ratio were found to moderately increase the column moment capacity. For instance, an increase from 0.70% to 1.25% longitudinal reinforcement for UHPC at an axial load ratio of 10% only increased the nominal moment capacity by 13% despite a near doubling of the reinforcement ratio. In addition, moderate increases in drift capacity with increasing reinforcement ratio can also be observed when comparing Figures 2a and 2c and Figures 2b and 2d, respectively.







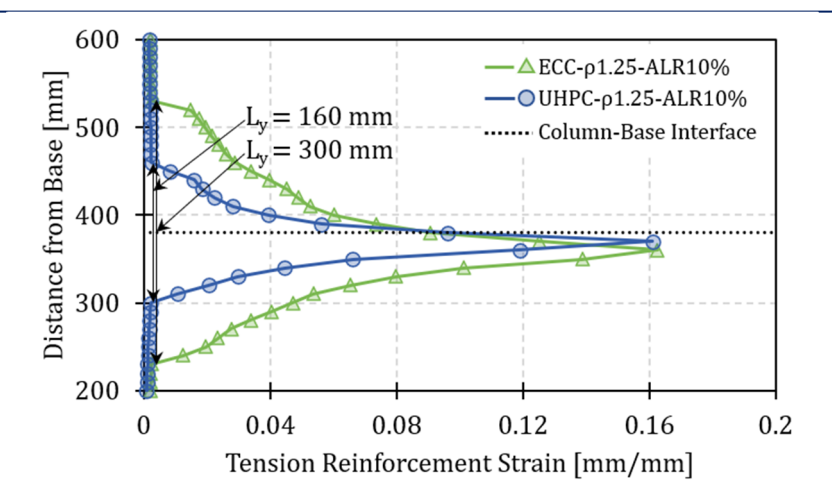


Figure 3: Distance from base of column versus tension reinforcement strain before failure drift for ECC-ρ1.25-ALR10% and UHPC-ρ1.25-ALR10%.

Despite UHPC's significantly higher tensile strength, ECC columns generally had double the drift capacity of UHPC columns. This may be attributed to the inherent high bond stresses and strain compatibility associated with high material tensile strengths (Fischer & Li, 2003) which can result in reinforcement plastic straining over a smaller length (Moreno et al., 2014). To investigate the effects of bond strength on component drift capacity, reinforcement strains for ECC and UHPC at failure were extracted, and the length (L_y) over which plastic straining occurred was measured as shown in Figure 3. It can be observed that the plastic straining length of UHPC, 160 mm, is nearly half of the length of ECC, 300 mm. The observed trends in smaller distributed plasticity in reinforcement with higher bond strengths further align with experimental tension stiffening tests (Moreno et al., 2014).

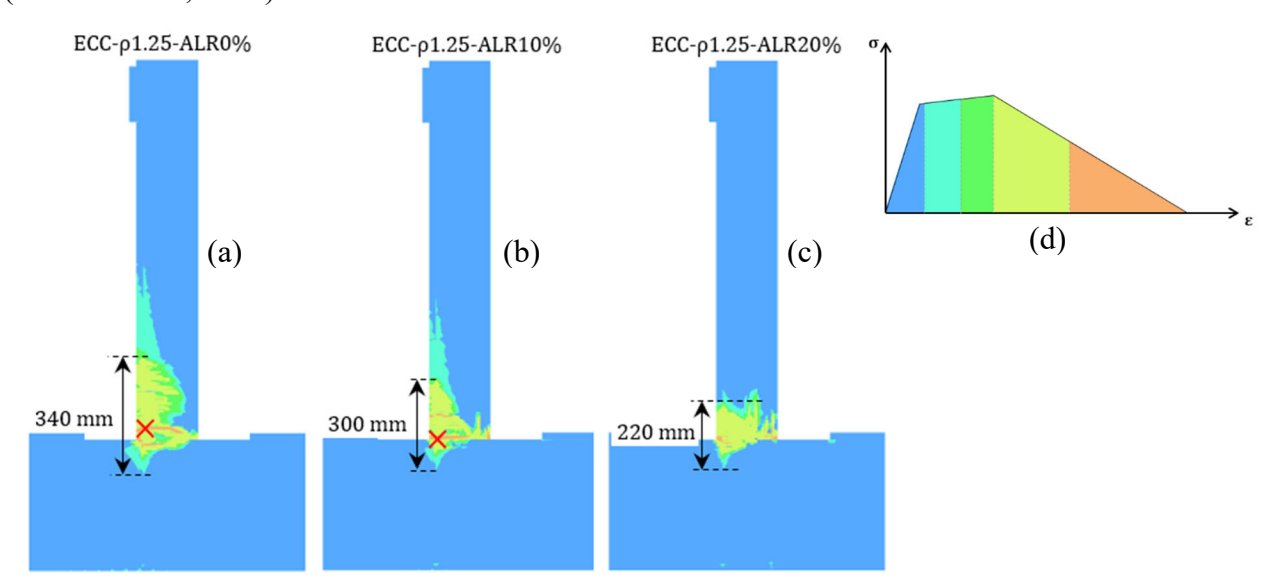


Figure 4: Principle tensile strains for (a) ECC-\rho1.25%-ALR0%, (b) ECC-\rho1.25%-ALR10%, and (c) ECC-\rho1.25%-ALR20%. (d) Principle tensile strain contour key. × indicates the location of tensile reinforcement fracture.







To evaluate the change in damage patterns and failure modes, the principle tensile strain contours at failure for three representative simulations are presented in Figure 4. For ECC-p1.25%-ALR0%, two localized cracks formed above and below the column-foundation interface with plastic softening damage – associated with fiber pullout and rupture – penetrating across the majority of the cross-section. For ECC-p1.25%-ALR10%, two localized cracks formed at and above the column-foundation interface. The length over which plastic softening damage occurred decreased from 340 mm to 300 mm and more gradual cross-sectional damage was observed. In addition, the increased damage and thus engagement of the compression side. Lastly, for ECC-p1.25%-ALR20%, one small localized crack formed and penetrated only 20 mm into the column section. Plastic damage at this load level was observed to be distributed across the base of the column and may imply a partial combination of horizontal damage from flexure and vertical damage from compression.

4 Conclusions

In this study, the influence of material properties, reinforcement ratios, and axial load level on R/HPFRCC column behavior was investigated through numerical simulations. It was observed that axial load can considerably increase the nominal moment capacity of R/HPFRCC columns as well as affect the drift capacity and failure mechanisms. In addition, it was observed that UHPC had higher flexural strengths, but failed at lower drift levels than ECC despite its greater tensile strength. Comparisons of ECC and UHPC tensile strains illustrated how the changes in bond stress due to changing material tensile strength explain the considerable differences in component drift capacities. Lastly, the evaluation of the principle tensile strains at different axial load levels further elucidated the observed trends in the moment-drift responses and changes in failure mechanisms.

Future research efforts should investigate the effects of biaxial stress states on material response as this study was limited by an "unconfined" compressive stress-strain model that did not account for transverse reinforcement contributions. In addition, efforts should be made to 1) report sufficient experimental information to help further progress numerical models and 2) investigate the minimum fiber, longitudinal, and transverse reinforcement to obtain a guaranteed drift capacity and damage level.

5 Acknowledgments

This material is based upon work supported by the National Science Foundation under Grant No. 2141955. Any opinions, findings, conclusions, or recommendations expressed in this material are those of the author(s) and do not necessarily reflect the views of the National Science Foundation.

6 References

Aboukifa, M., & Moustafa, M. A. (2021). Experimental seismic behavior of ultra-high performance concrete columns with high strength steel reinforcement. *Engineering Structures*, 232. https://doi.org/10.1016/j.engstruct.2021.111885







- Bandelt, M. J., & Billington, S. L. (2016a). Bond behavior of steel reinforcement in high-performance fiber-reinforced cementitious composite flexural members. *Materials and Structures*, 49(1–2), 71–86. https://doi.org/10.1617/s11527-014-0475-4
- Bandelt, M. J., & Billington, S. L. (2016b). Impact of Reinforcement Ratio and Loading Type on the Deformation Capacity of High-Performance Fiber-Reinforced Cementitious Composites Reinforced with Mild Steel. *Journal of Structural Engineering*, 142(10). https://doi.org/10.1061/(asce)st.1943-541x.0001562
- Bandelt, M. J., & Billington, S. L. (2018). Simulation of Deformation Capacity in Reinforced High-Performance Fiber-Reinforced Cementitious Composite Flexural Members. *Journal of Structural Engineering*, 144(10), 04018188. https://doi.org/10.1061/(asce)st.1943-541x.0002174
- Chao, S. H., Shamshiri, M., Liu, X., Palacios, G., Schultz, A. E., & Nojavan, A. (2021). Seismically robust ultra-high-performance fiber-reinforced concrete columns. *ACI Structural Journal*, 118(2), 17–32. https://doi.org/10.14359/51730391
- Fischer, G., & Li, V. C. (2003). Effect of Matrix Ductility on Deformation Behavior of Steel-Reinforced ECC Flexural Members under Reversed Cyclic Loading Conditions. *ACI Structural Journal*, 99(6), 781–790.
- Frank, T. E., Lepech, M. D., & Billington, S. L. (2017). Experimental testing of reinforced concrete and reinforced ECC flexural members subjected to various cyclic deformation histories. *Materials and Structures/Materiaux et Constructions*, 50(5). https://doi.org/10.1617/s11527-017-1102-y
- Graybeal, B. A. (2006). *Material Property Characterization of Ultra-High Performance Concrete*. Hung, C. C., Hu, F. Y., & Yen, C. H. (2018). Behavior of slender UHPC columns under eccentric loading. *Engineering Structures*, 174, 701–711. https://doi.org/10.1016/j.engstruct.2018.07.088
- Li, L. Z., Bai, Y., Yu, K. Q., Yu, J. T., & Lu, Z. D. (2019). Reinforced high-strength engineered cementitious composite (ECC) columns under eccentric compression: Experiment and theoretical model. *Engineering Structures*, 198. https://doi.org/10.1016/j.engstruct.2019.109541
- Marchand, P., Baby, F., Khadour, A., Rivillon, P., Renaud, J.-C., Baron, L., Généreux, G., Deveaud, J.-P., Simon, A., & Toutlemonde, F. (2019). Response of UHPFRC Columns Submitted to Combined Axial and Alternate Flexural Loads. *Journal of Structural Engineering*, 145(1). https://doi.org/10.1061/(asce)st.1943-541x.0002209
- Moreno, D. M., Trono, W., Jen, G., Ostertag, C., & Billington, S. L. (2014). Tension stiffening in reinforced high performance fiber reinforced cement-based composites. *Cement and Concrete Composites*, 50, 36–46. https://doi.org/10.1016/j.cemconcomp.2014.03.004
- Naaman, A. E., & Reinhardt, H. W. (2006). Proposed classification of HPFRC composites based on their tensile response. *Materials and Structures/Materiaux et Constructions*, 39(5), 547–555. https://doi.org/10.1617/s11527-006-9103-2
- Paulay, T., & Priestley, M. J. N. (1992). Seismic Design of Reinforced Concrete and Masonry Buildings. John Wiley & Sons, Inc.
- Pokhrel, M., & Bandelt, M. J. (2019). Material properties and structural characteristics influencing deformation capacity and plasticity in reinforced ductile cement-based composite structural components. *Composite Structures*, 224. https://doi.org/10.1016/j.compstruct.2019.111013







- Rots, J. G. (1988). *Computational Modeling of Concrete Fracture* [Delft University of Technology]. https://repository.tudelft.nl/islandora/object/uuid%3A06985d0d-1230-4a08-924a-2553a171f08f
- Russell, H. G., & Graybeal, B. A. (2013). *Ultra-High Performance Concrete: A State-of-the-Art Report for the Bridge Community*. https://www.fhwa.dot.gov/publications/research/infrastructure/structures/hpc/13060/13060.pdf
- Shao, Y., Asce, A. M., Hung, C.-C., Asce, M., & Billington, S. L. (2021). *Gradual Crushing of Steel Reinforced HPFRCC Beams: Experiments and Simulations*. https://doi.org/10.1061/(ASCE)
- Shao, Y., & Billington, S. L. (2022). Impact of UHPC Tensile Behavior on Steel Reinforced UHPC Flexural Behavior. *Journal of Structural Engineering*, 148(1). https://doi.org/10.1061/(asce)st.1943-541x.0003225
- Shao, Y., Nguyen, W., Bandelt, M. J., Ostertag, C. P., & Billington, S. L. (2022). Seismic Performance of High-Performance Fiber-Reinforced Cement-Based Composite Structural Members: A Review. *Journal of Structural Engineering*, 148(10). https://doi.org/10.1061/(asce)st.1943-541x.0003428
- Shao, Y., & Ostertag, C. P. (2022). Bond-slip behavior of steel reinforced UHPC under flexure: Experiment and prediction. *Cement and Concrete Composites*, 133. https://doi.org/10.1016/j.cemconcomp.2022.104724
- Tariq, H., Jampole, E. A., & Bandelt, M. J. (2021). Development and Application of Spring Hinge Models to Simulate Reinforced Ductile Concrete Structural Components under Cyclic Loading. *Journal of Structural Engineering*, 147(2). https://doi.org/10.1061/(asce)st.1943-541x.0002891
- Wille, K., El-Tawil, S., & Naaman, A. E. (2014). Properties of strain hardening ultra high performance fiber reinforced concrete (UHP-FRC) under direct tensile loading. *Cement and Concrete Composites*, 48, 53–66. https://doi.org/10.1016/j.cemconcomp.2013.12.015
- Willie, K., & Naaman, A. E. (2010). Fracture energy of UHP-FRC under direct tensile loading. *Fracture Mechanics of Concrete and Concrete Structures*, 65–72.
- Wu, C., Pan, Z., Su, R. K. L., Leung, C. K. Y., & Meng, S. (2017). Seismic behavior of steel reinforced ECC columns under constant axial loading and reversed cyclic lateral loading. *Materials and Structures/Materiaux et Constructions*, 50(1). https://doi.org/10.1617/s11527-016-0947-9
- Xu, S., Wu, C., Liu, Z., Han, K., Su, Y., Zhao, J., & Li, J. (2017). Experimental investigation of seismic behavior of ultra-high performance steel fiber reinforced concrete columns. *Engineering Structures*, 152, 129–148. https://doi.org/10.1016/j.engstruct.2017.09.007
- Yoo, D. Y., & Yoon, Y. S. (2015). Structural performance of ultra-high-performance concrete beams with different steel fibers. *Engineering Structures*, 102, 409–423. https://doi.org/10.1016/j.engstruct.2015.08.029